JOURNAL OF THE AMERICAN CHEMICAL SOCIETY

# Control of Intermolecular Bonds by Deposition Rates at Room Temperature: Hydrogen Bonds versus Metal Coordination in Trinitrile Monolayers

Thomas Sirtl,[†,‡] Stefan Schlögl,[†,‡] Atena Rastgoo-Lahrood,[†,‡] Jelena Jelic,[§] Subhadip Neogi,[∥] Michael Schmittel,[∥] Wolfgang M. Heckl,[†,‡,⊥] Karsten Reuter,[§] and Markus Lackinger*[,‡,⊥]

[†]Department of Physics, Technische Universität München, James-Franck-Str. 1, 85748 Garching, Germany
[‡]Center for NanoScience (CeNS), Schellingstr. 4, 80799 Munich, Germany
[§]Department of Chemistry, Technische Universität München, Lichtenbergstr. 4, 85747 Garching, Germany
[∥]Center of Micro- and Nanochemistry and Engineering, Organische Chemie I, Universität Siegen, Adolf-Reichwein-Str. 2, 57068 Siegen, Germany
[⊥]Deutsches Museum, Museumsinsel 1, 80538 Munich, Germany

*Supporting Information*

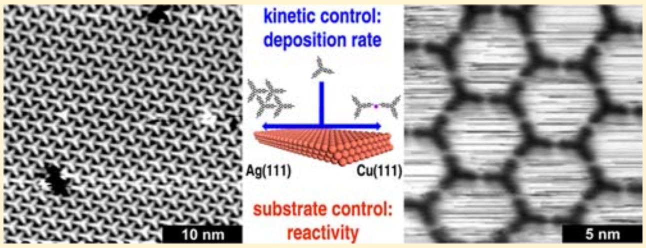

**ABSTRACT:** Self-assembled monolayers of 1,3,5-tris(4′-biphenyl-4″-carbonitrile)benzene, a large functional trinitrile molecule, on the (111) surfaces of copper and silver under ultrahigh vacuum conditions were studied by scanning tunneling microscopy and low-energy electron diffraction. A densely packed hydrogen-bonded polymorph was equally observed on both surfaces. Additionally, deposition onto Cu(111) yielded a well-ordered metal-coordinated porous polymorph that coexisted with the hydrogen-bonded structure. The required coordination centers were supplied by the adatom gas of the Cu(111) surface. On Ag(111), however, the well-ordered metal-coordinated network was not observed. Differences between the adatom reactivities on copper and silver and the resulting bond strengths of the respective coordination bonds are held responsible for this substrate dependence. By utilizing ultralow deposition rates, we demonstrate that on Cu(111) the adatom kinetics plays a decisive role in the expression of intermolecular bonds and hence structure selection.

## INTRODUCTION

Self-assembled organic monolayers are promising candidates for the development of novel materials with tremendous options.[1] Many of their properties decisively depend on the type of intermolecular bond that stabilizes the monolayer.[2] The bond type is mostly predetermined by functionalization but may additionally be influenced by kinetic effects. For instance, temperature can affect structure formation because of activation barriers.[3,4] Among the different non-covalent intermolecular bonds that can stabilize monolayers, not only is metal coordination the strongest,[5] but thiolate−copper coordination bonds, for example, can also offer strong intermolecular electronic coupling as required for molecular electronic applications.[6]

Formation of metal-coordination bonds requires both electron-donating ligands and metal centers. For surface-supported systems, the latter can be supplied either by metal deposition or by the adatom gas of a metal surface. Deposition of extrinsic metal centers facilitates chemical variability, while network formation with intrinsic metal centers offers facile preparation. Carboxylates and thiolates are suitable anionic ligands for coordinative bonds,[2,6−8] while nitrogen in heterocycles (e.g., pyridine or other azines) or nitriles are among the favored neutral ligands.[2,5,9,10] In contrast to thiol and carboxyl groups, where the formation of metal-coordinated networks requires additional thermal activation,[2,6,8] nitrile coordination is readily observed at room temperature with an onset around 180 K.[3]

For many correspondingly functionalized molecules, the type of intermolecular bond can be changed by supplying coordination centers. A good example therefore are dinitriles on Ag(111).[5,9,11−13] Additional deposition of cobalt atoms induces a change from hydrogen bonding to metal coordination, accompanied by structural reorganization.

Besides temperature, the competition between molecular flux onto the surface and diffusion on the surface can also play a decisive kinetic role in determining the structure. An experimental example is given by Li and Lin,[14] who observed structurally different pyridyl−porphyrin monolayers upon variation of the deposition rate. However, all of these structures were stabilized by the same type of intermolecular bond (i.e.,

**Received:** July 13, 2012
**Published:** December 18, 2012

dx.doi.org/10.1021/ja306834a | *J. Am. Chem. Soc.* 2013, 135, 691−695

copper coordination), and no change of bond type was induced.

Here we studied the self-assembly of the large functional molecule 1,3,5-tris(4′-biphenyl-4″-carbonitrile)benzene (BCNB) on both Cu(111) and Ag(111). These surfaces were chosen as substrates because they exhibit two-dimensional adatom gases that are comparable in mobility[15] but differ in reactivity.[4,16] To study the influence of the above-mentioned kinetic competition on the formation of adatom-coordinated trinitrile networks, experiments were conducted with variation of the deposition rate over two orders of magnitude.

## ■ EXPERIMENTAL DETAILS

BCNB monolayers were characterized by scanning tunneling microscopy (STM) and low-energy electron diffraction (LEED) in ultrahigh vacuum (UHV). STM data were acquired with a home-built beetle-type scanning tunneling microscope driven by an SPM100 controller from RHK. The topographs were processed by a mean value filter. All of the images were obtained at room temperature at a base pressure below $3 \times 10^{-10}$ mbar. The Ag(111) and Cu(111) single-crystal surfaces were prepared by cycles of $Ne^+$ ion sputtering at 1 keV and electron-beam annealing at 550 °C for 30 min. Thorough calibration of the microscope with atomically resolved topographs of Cu(111) allowed lattice parameters and distances to be derived with an accuracy of ~5%.

LEED experiments were performed in a separate UHV chamber at a base pressure below $1 \times 10^{-10}$ mbar. The LEED optics (Omicron NanoTechnology GmbH) were controlled by electronics from SPECS Surface Nano Analysis GmbH. The Ag(111) and Cu(111) surfaces were prepared by $Ar^+$ ion sputtering at 2 keV and subsequent electron-beam annealing at 550 °C for 30 min. The deposition parameters were similar to those for the STM experiments. LEED patterns were acquired at a sample temperature of ~60 K. The software LEEDpat3 was used for geometric simulations.

BCNB (see the Figure 1 inset for its molecular structure and the Supporting Information for its synthesis) was deposited from a home-built Knudsen cell[17] and thoroughly outgassed prior to deposition. The substrates were held at room temperature. The crucible temperature was varied between 280 and 330 °C, resulting in deposition rates between $\sim 2.5 \times 10^{-4}$ and $\sim 2.5 \times 10^{-2}$ monolayer/min, respectively. To determine the BCNB sublimation rate as a function of crucible temperature and to verify the long-term stability of the sublimation, a Knudsen cell equipped with a quartz crystal microbalance was used.[18]

## ■ RESULTS AND DISCUSSION

On Ag(111), BCNB self-assembles into long-range-ordered, densely packed monolayers with *p*31*m* symmetry. Both STM and LEED consistently revealed a $(\sqrt{39}\times\sqrt{39})\mathrm{R}\pm16°$ superstructure with a lattice parameter of 1.80 nm (Figure 1). The existence of two rotational domains is evident in the LEED pattern depicted in the lower inset.[18] The identification of the molecular arrangement is unambiguous since the threefold contour of BCNB is clearly recognizable and the STM-derived size is in excellent agreement with the optimized geometry of the isolated BCNB molecule.[18] On the basis of the dense packing of BCNB, additional constituents can be excluded. From the molecular arrangement, it is concluded that the dominant interactions are C≡N···H−C hydrogen bonds, as similarly observed in surface self-assembly[3,11,19] and bulk crystals[20,21] of carbonitriles. The nitrile groups are in close proximity to three phenyl hydrogen atoms. Density functional theory (DFT) calculations of two isolated molecules gave a center-to-center distance of 1.81 nm.[18] The extremely small deviation from the experiment (1.80 nm) indicates a minor substrate influence and justifies the comparison with gas-phase calculations. The closest N···H distances (260 pm) are consistent with hydrogen-bond lengths in comparable bulk crystals (250−260 pm).[20,21]

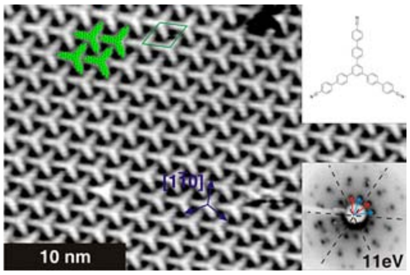

**Figure 1.** STM topograph (+1.61 V, 100 pA) of the densely packed $(\sqrt{39}\times\sqrt{39})\mathrm{R}\pm16°$ BCNB superstructure on Ag(111). Molecules are overlaid, and the unit cell is indicated by green lines. The structure of BCNB is shown in the upper inset. The lower inset shows the LEED pattern. The two rotational domains are marked by red and turquoise arrows.[18] Dashed lines indicate high-symmetry substrate directions.

BCNB deposition with a rate of $\sim 2.5 \times 10^{-2}$ monolayer/min onto Cu(111) yielded two polymorphs, both with *p*31*m* symmetry. The overview STM image in Figure 2a illustrates the coexistence of both a densely packed *α* phase and a porous *β* phase. The lattice parameter and molecular arrangement of the *α* phase on Cu(111) are comparable to those on Ag(111). The commensurate $(4\sqrt{3}\times4\sqrt{3})\mathrm{R}30°$ superstructure on Cu(111) (cf. the Figure 2a inset for the LEED pattern)[18] exhibits a slightly smaller lattice parameter of 1.77 nm and only one rotational domain. According to the similarities with the structure on Ag(111), it is concluded that the *α* phase on Cu(111) is likewise stabilized by similar intermolecular C≡N···H−C hydrogen bonds.

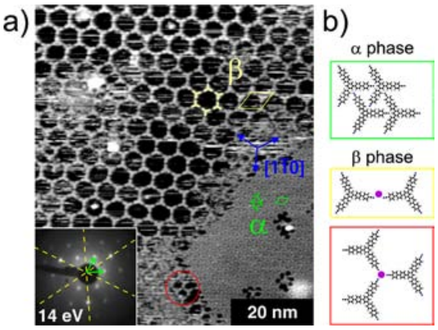

**Figure 2.** (a) STM topograph (+2.09 V, 80 pA) of a BCNB monolayer on Cu(111) deposited at a rate of $\sim 2.5 \times 10^{-2}$ monolayer/min. The inset shows the LEED pattern,[18] in which arrows indicate the reciprocal unit cell vectors of the *α* phase and dashed lines mark high-symmetry substrate directions. (b) Tentative binding models of the *α* (green) and *β* (yellow) phases; threefold coordination (red) was also occasionally observed, but only in isolated arrangements.

The pores of the *β* phase are arranged on a hexagonal lattice, and the unit cell contains two molecules. The streaky features observed within some but not all of the pores arise from entrapped mobile species, either excess molecules or adatoms. Similar observations have been reported for various porous systems.[11,22−25] Two different epitaxial relations to the substrate were found, namely, $(11\sqrt{3}\times11\sqrt{3})\mathrm{R}\pm30°$ and 19×19 superstructures having almost identical lattice parameters (4.87 and 4.86 nm, respectively). Generally, the emergence of a porous polymorph already hints at stronger intermolecular bonds. From the rather large center-to-center distance of 2.8 nm between adjacent molecules, direct interactions via intermolecular hydrogen bonds can a priori be excluded. A detailed view of the *β* phase furthermore revealed an arrangement where the molecular lobes are not aligned with the long diagonal of the unit cell but are slightly tilted by ±9° (Figure 3). In most dimeric binding motifs, the two molecules tilt in the same direction (i.e., one molecule tilts clockwise and the other counterclockwise). Tilts can occur in both directions and occur in segregated domains.[18]

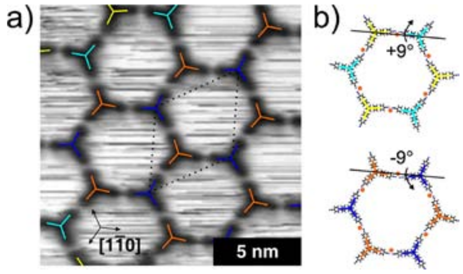

**Figure 3.** *β* phase of BCNB on Cu(111). (a) Close-up STM topograph (1.41 V, 80 pA) with overlaid tripods. The colors encode the different tilts of ±9°. (b) Tentative models. C, gray; Cu, orange; H, white; N, blue.

On the basis of the intermolecular arrangement, we propose that BCNB molecules are interconnected by coordination bonds between the nitrile groups and copper adatoms. This hypothesis is further substantiated by occasionally observed adatom-related contrast features in the STM images, the results of DFT calculations, and the good match with an epitaxial model, as detailed in the following. In accordance with most other experiments on copper-coordinated networks, the copper atoms are normally not resolved by STM.[26−32] This invisibility of obviously present coordination centers in STM images has also been reported for many other metal-coordinated networks, such as Co-coordinated nitriles[5,9,12,33] and is attributed to an electronic effect.[34] Nevertheless, occasionally for peculiar tip conditions, distinct topographic maxima were observed in the *β* phase at the proposed positions of the copper coordination centers (i.e., midway between two BCNB molecules; see the Supporting Information). Moreover, in these images, the BNCB molecules appear with diminished apparent height, indicating a tip that is sensitive to electronic states in a different energy range. Because of their positions, these topographic maxima are unambiguously identified as the coordinating copper adatoms. Similar signatures of coordinating adatoms in the STM contrast have been reported for Cu−benzoate complexes on Cu(110).[35]

In the *β* phase, copper adatoms coordinate two nitrile groups. Threefold coordination, the major binding motif in Co-coordinated nitrile networks[5,9,12] and hitherto-known Cu coordination,[3] was only rarely observed in isolated arrangements (Figure 2). However, for surface-supported metal-coordinated networks, unusual coordination with lower coordination numbers seems to be the more general case.[8,27,36] This can be rationalized by the special environment of these surface-supported systems. On the one hand, there is the restriction to a planar geometry due to the surface confinement, and on the other hand, there is an additional electronic influence of the metal surface due to charge transfer and screening by free electrons.[27,36]

DFT calculations were performed to derive optimal bond lengths for copper−nitrile coordination and to find explanations for the tilt in the intermolecular bonds. For a full account of surface effects, it is also important to include the copper substrate. However, because of the large system size, the DFT calculations had to be restricted to benzonitrile as a representative model system. As depicted in Figure 4a, energy minimization of two benzonitrile molecules coordinated to one copper adatom resulted in a straight bond with the adatom stably adsorbed in a threefold hollow site. The N−Cu bond length is 0.192 nm, and the copper adatom resides 0.200 nm above the topmost copper layer and 0.121 nm below the benzene rings. The DFT calculations revealed a global energy minimum for the benzene rings oriented along the $\langle 1\bar{1}0\rangle$ high-symmetry direction of the substrate and a further, only slightly less stable local minimum for alignment in the bisecting $\langle 11\bar{2}\rangle$ direction.

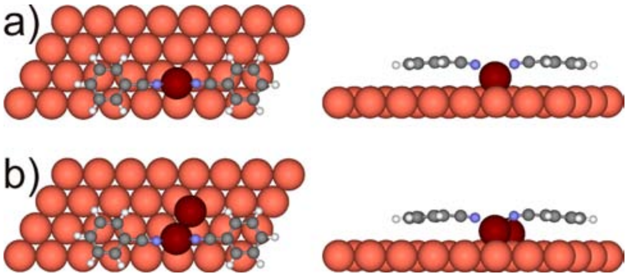

**Figure 4.** DFT geometry optimization of two benzonitrile molecules coordinated to copper adatoms (represented by dark-red spheres). Left: top views (i.e., parallel to [111]). Right: side views (i.e., parallel to $[11\bar{2}]$). Only one copper substrate layer is depicted, but three layers were considered in the calculation. (a) Coordination to one copper adatom in a threefold hollow site. (b) Coordination to one copper adatom in a threefold hollow site with a further copper adatom in an adjacent site.

Since DFT geometry optimization yielded a straight bond, the experimentally observed tilt cannot be explained by intrinsic properties of the chosen model system. In an alternative approach, a second copper adatom was placed adjacent to the coordinating copper atom, likewise in a threefold hollow site. The optimized geometry is depicted in Figure 4b. Addition of a second adatom actually results in a tilt of the bond angle by 6°, thereby offering a possible explanation.

Although the DFT simulations of the model systems included direct substrate effects, conceivable registry effects could arise for the full BCNB molecule that could be relevant for the *β* phase. Nevertheless, an optimal N−Cu bond length of 0.192 nm in the adsorbed system was deduced from the DFT calculations, and there is a clear confirmation that copper adatoms have a strong preference for threefold hollow sites. The fairly large unit cell of the *β* phase contains two BCNB molecules and three copper adatoms. When the above-stated requirements are considered, it becomes clear that the substrate registry does not allow for a straight bond configuration. To keep $C\equiv N-Cu$ coordination bonds within 5% of the optimized length and guarantee threefold hollow sites for all adatoms, the *β* phase has to adapt to the substrate lattice in the energetically most efficient way, which involves tilting the BCNB molecules with respect to each other. A tentative model of the *β* phase that includes all of the requirements and the experimental tilt angle into account is presented in Figure 5.

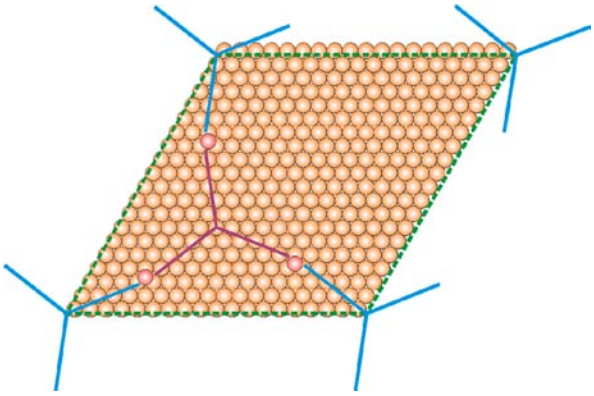

**Figure 5.** Tentative model of the $\beta$ phase on Cu(111). The dashed green lines indicate the 19×19 unit cell. For clarity, the BCNB molecules are represented by tripods. This model considers the experimental tilt angle and the preference of copper adatoms for threefold hollow sites. All C≡N−Cu bonds are within 5% of the DFT-derived optimal bond length of 0.192 nm. The three coordinating copper adatoms are located on the same sublattice.[18]

To obtain insights into the growth kinetics, experiments were conducted with ultraslow deposition, wherein a surface coverage of one monolayer was accomplished in 67 h. On Cu(111), this resulted in the exclusive formation of the $\beta$ phase, thereby hinting at a kinetic origin of the polymorphism. A representative STM image is presented in Figure 6a. Irrespective of the low deposition rate, a similar tilt angle between the BCNB molecules was observed, pointing to an equilibrium effect. Occasionally, the STM images also showed a parallel side-by-side arrangement of two dimers, an example of which is highlighted in Figure 6a. However, these uncommon coordination schemes are grouped along a line and thus are attributed to an antiphase domain boundary. Interestingly, similarly slow deposition onto Ag(111) still resulted in the densely packed polymorph, yet with a notably extended domain size, as illustrated in Figure 6b.

We thus assign the polymorphism on Cu(111) to a kinetic effect, namely, the availability of Cu adatoms. Upon deposition of BCNB, formation of the $\beta$ phase consumes Cu adatoms and thus depletes the density of the adatom gas below its equilibrium value. If the progressive consumption of Cu adatoms caused by further deposition of BCNB molecules is faster than adatom replenishment from step edges, the availability of Cu centers for coordination bonds decreases. The absence of Cu adatoms leads to the realization of the second best option in terms of intermolecular bonds, namely, the hydrogen-bonded $\alpha$ phase.

This picture is supported by the experiments on Cu(111) with ultraslow deposition, which resulted in the exclusive formation of the $\beta$ phase. When the BCNB deposition rate is so low that the equilibrium density of the adatom gas is not perturbed, Cu centers are constantly available, and the preferred formation of Cu coordination bonds is not hampered by kinetic limitations. In contrast, the insufficient reactivity of Ag adatoms at room temperature leads to the exclusive formation of the hydrogen-bonded structure on Ag(111), even for ultraslow deposition. On this less reactive surface, the slow deposition affects only the nucleation and growth kinetics, resulting in extended domains of the densely packed hydrogen-bonded phase.

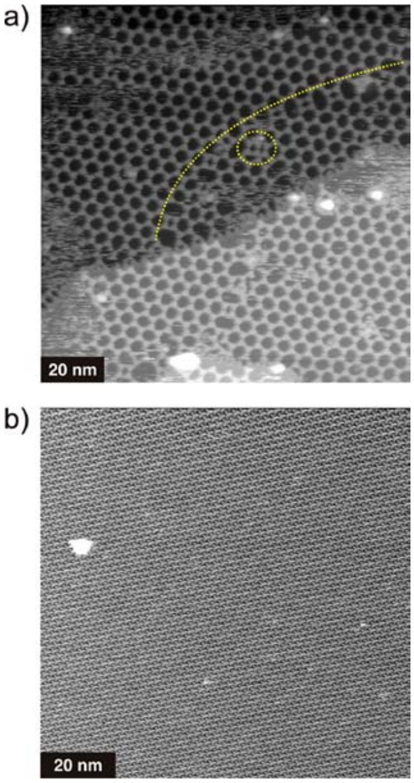

**Figure 6.** (a) STM topograph (+2.01 V, 39 pA) of BCNB on Cu(111). The monolayer was prepared by ultraslow deposition (~2.5 × $10^{-4}$ monolayer/min), which exclusively yielded the porous $\beta$ phase. The dashed circle highlights a parallel side-by-side arrangement of dimers, and the dashed line indicates a domain boundary. (b) STM topograph (−0.19 V, 40 pA) of BCNB on Ag(111). The monolayer was similarly prepared by ultraslow deposition (~8.3 × $10^{-4}$ monolayer/min). However, on Ag(111) no change of intermolecular bond type was induced. The $\alpha$ phase was observed exclusively but with a notably increased domain size.

This striking difference between Cu(111) and Ag(111) can be explained by the lower bond dissociation energy (BDE) of C≡N−Ag vs C≡N−Cu coordination bonds. The BDE of two benzonitrile molecules coordinated either by one Cu atom or one Ag atom for isolated arrangements was evaluated by DFT calculations. The BDE for the copper case amounts to 0.90 eV per benzonitrile molecule, which is substantially higher than the value of 0.30 eV in the case of silver. Accordingly, Ag-coordinated BCNB networks might be stable only at lower temperature, although under those conditions the adatom density and mobility become the limiting factors for the formation of metal-coordinated networks.

## ■ CONCLUSION

The deposition-rate-dependent self-assembly of BCNB on Ag(111) and Cu(111) demonstrates the importance of both substrate and kinetic effects for the expression of a specific type of intermolecular bond. Two types of intermolecular bonds dominate in BCNB monolayers, namely, hydrogen bonds and metal-coordination bonds with adatoms. Their emergence can be controlled by the choice of substrate, a well-known effect that is in the case of metal coordination mostly related to the adatom reactivity and the bond strength of the respective coordination bonds. Moreover, here we discovered that the deposition rate is also effective in deliberately selecting the type of intermolecular bond and thus controlling the structure. A qualitative study of these kinetic effects allows for a basic understanding of growth kinetics and polymorph selection in the abundantly employed formation of metal−organic networks through adatom coordination.

## ASSOCIATED CONTENT

### Supporting Information

Synthesis details, curves showing the sublimation rate as functions of temperature and time, additional DFT calculations, STM and LEED data, and an additional structure model. This material is available free of charge via the Internet at http://pubs.acs.org.

## AUTHOR INFORMATION

### Corresponding Author

markus@lackinger.org

### Notes

The authors declare no competing financial interest.

## ACKNOWLEDGMENTS

Funding by the Fonds der Chemischen Industrie (T.S.), the Nanosystems-Initiative-Munich Cluster of Excellence, the Alexander von Humboldt Foundation (S.N.), and the Elitenetzwerk Bayern (S.S.) and discussions with Debabrata Samanta are gratefully acknowledged.

## REFERENCES

(1) Barth, J. V. *Annu. Rev. Phys. Chem.* **2007**, *58*, 375−407.

(2) Miyashita, N.; Kurth, D. G. *J. Mater. Chem.* **2008**, *18*, 2636−2649.

(3) Pawin, G.; Wong, K. L.; Kim, D.; Sun, D. Z.; Bartels, L.; Hong, S.; Rahman, T. S.; Carp, R.; Marsella, M. *Angew. Chem., Int. Ed.* **2008**, *47*, 8442−8445.

(4) Walch, H.; Gutzler, R.; Sirtl, T.; Eder, G.; Lackinger, M. *J. Phys. Chem. C* **2010**, *114*, 12604−12609.

(5) Bartels, L. *Nat. Chem.* **2010**, *2*, 87−95.

(6) Walch, H.; Dienstmaier, J.; Eder, G.; Gutzler, R.; Schlögl, S.; Sirtl, T.; Das, K.; Schmittel, M.; Lackinger, M. *J. Am. Chem. Soc.* **2011**, *133*, 7909−7915.

(7) Lin, N.; Dmitriev, A.; Weckesser, J.; Barth, J. V.; Kern, K. *Angew. Chem., Int. Ed.* **2002**, *41*, 4779−4783.

(8) Lin, N.; Stepanow, S.; Vidal, F.; Kern, K.; Alam, M. S.; Strömsdörfer, S.; Dremov, V.; Müller, P.; Landa, A.; Ruben, M. *Dalton Trans.* **2006**, 2794−2800.

(9) Schlickum, U.; Klappenberger, F.; Decker, R.; Zoppellaro, G.; Klyatskaya, S.; Ruben, M.; Kern, K.; Brune, H.; Barth, J. V. *J. Phys. Chem. C* **2010**, *114*, 15602−15606.

(10) Schütte, M.; Kurth, D. G.; Linford, M. R.; Cölfen, H.; Möhwald, H. *Angew. Chem., Int. Ed.* **1998**, *37*, 2891−2893.

(11) Kühne, D.; Klappenberger, F.; Decker, R.; Schlickum, U.; Brune, H.; Klyatskaya, S.; Ruben, M.; Barth, J. V. *J. Phys. Chem. C* **2009**, *113*, 17851−17859.

(12) Klyatskaya, S.; Klappenberger, F.; Schlickum, U.; Kuhne, D.; Marschall, M.; Reichert, J.; Decker, R.; Krenner, W.; Zoppellaro, G.; Brune, H.; Barth, J. V.; Ruben, M. *Adv. Funct. Mater.* **2011**, *21*, 1230−1240.

(13) Kühnle, A. *Curr. Opin. Colloid Interface Sci.* **2009**, *14*, 157−168.

(14) Li, Y.; Lin, N. *Phys. Rev. B* **2011**, *84*, No. 125418.

(15) Agrawal, P. M.; Rice, B. M.; Thompson, D. L. *Surf. Sci.* **2002**, *515*, 21−35.

(16) Lin, N.; Payer, D.; Dmitriev, A.; Strunskus, T.; Wöll, C.; Barth, J. V.; Kern, K. *Angew. Chem., Int. Ed.* **2005**, *44*, 1488−1491.

(17) Gutzler, R.; Heckl, W. M.; Lackinger, M. *Rev. Sci. Instrum.* **2010**, *81*, No. 015108.

(18) See the Supporting Information.

(19) Yokoyama, T.; Yokoyama, S.; Kamikado, T.; Okuno, Y.; Mashiko, S. *Nature* **2001**, *413*, 619−621.

(20) Özbey, S.; Kaynak, F. B.; Göker, H.; Kus, C. *J. Chem. Crystallogr.* **2004**, *34*, 851−858.

(21) Döpp, D.; Kruse, C.; Flörke, U.; Henkel, G. *Acta Crystallogr., Sect. E* **2006**, *62*, O3245−O3246.

(22) Griessl, S.; Lackinger, M.; Edelwirth, M.; Hietschold, M.; Heckl, W. M. *Single Mol.* **2002**, *3*, 25−31.

(23) Ruben, M.; Payer, D.; Landa, A.; Comisso, A.; Gattinoni, C.; Lin, N.; Collin, J. P.; Sauvage, J. P.; De Vita, A.; Kern, K. *J. Am. Chem. Soc.* **2006**, *128*, 15644−15651.

(24) Otero, R.; Lukas, M.; Kelly, R. E. A.; Xu, W.; Laegsgaard, E.; Stensgaard, I.; Kantorovich, L. N.; Besenbacher, F. *Science* **2008**, *319*, 312−315.

(25) Stöhr, M.; Wahl, M.; Galka, C. H.; Riehm, T.; Jung, T. A.; Gade, L. H. *Angew. Chem., Int. Ed.* **2005**, *44*, 7394−7398.

(26) Classen, T.; Lingenfelder, M.; Wang, Y.; Chopra, R.; Virojanadara, C.; Starke, U.; Costantini, G.; Fratesi, G.; Fabris, S.; de Gironcoli, S.; Baroni, S.; Haq, S.; Raval, R.; Kern, K. *J. Phys. Chem. A* **2007**, *111*, 12589−12603.

(27) Heim, D.; Écija, D.; Seufert, K.; Auwärter, W.; Aurisicchio, C.; Fabbro, C.; Bonifazi, D.; Barth, J. V. *J. Am. Chem. Soc.* **2010**, *132*, 6783−6790.

(28) Tait, S. L.; Langner, A.; Lin, N.; Stepanow, S.; Rajadurai, C.; Ruben, M.; Kern, K. *J. Phys. Chem. C* **2007**, *111*, 10982−10987.

(29) Matena, M.; Stöhr, M.; Riehm, T.; Björk, J.; Martens, S.; Dyer, M. S.; Persson, M.; Lobo-Checa, J.; Müller, K.; Enache, M.; Wadepohl, H.; Zegenhagen, J.; Jung, T. A.; Gade, L. H. *Chem.—Eur. J.* **2010**, *16*, 2079−2091.

(30) Wang, Y.; Fabris, S.; White, T. W.; Pagliuca, F.; Moras, P.; Papagno, M.; Topwal, D.; Sheverdyaeva, P.; Carbone, C.; Lingenfelder, M.; Classen, T.; Kern, K.; Costantini, G. *Chem. Commun.* **2011**, *48*, 534−536.

(31) Björk, J.; Matena, M.; Dyer, M. S.; Enache, M.; Lobo-Checa, J.; Gade, L. H.; Jung, T. A.; Stöhr, M.; Persson, M. *Phys. Chem. Chem. Phys.* **2010**, *12*, 8815−8821.

(32) Matena, M.; Riehm, T.; Stöhr, M.; Jung, T. A.; Gade, L. H. *Angew. Chem., Int. Ed.* **2008**, *47*, 2414−2417.

(33) Schlickum, U.; Decker, R.; Klappenberger, F.; Zoppellaro, G.; Klyatskaya, S.; Ruben, M.; Silanes, I.; Arnau, A.; Kern, K.; Brune, H.; Barth, J. V. *Nano Lett.* **2007**, *7*, 3813−3817.

(34) Classen, T.; Fratesi, G.; Costantini, G.; Fabris, S.; Stadler, F. L.; Kim, C.; de Gironcoli, S.; Baroni, S.; Kern, K. *Angew. Chem., Int. Ed.* **2005**, *44*, 6142−6145.

(35) Dougherty, D. B.; Maksymovych, P.; Yates, J. T., Jr. *Surf. Sci.* **2006**, *600*, 4484−4491.

(36) Stepanow, S.; Lin, N.; Payer, D.; Schlickum, U.; Klappenberger, F.; Zoppellaro, G.; Ruben, M.; Brune, H.; Barth, J. V.; Kern, K. *Angew. Chem., Int. Ed.* **2007**, *46*, 710−713.